Fast Generation of GHZ-like States Using Collective-Spin XYZ Model

Xuanchen Zhang,[1,*] Zhiyao Hu,[2,1,*] and Yong-Chun Liu[1,3,†]

[1]*State Key Laboratory of Low-Dimensional Quantum Physics, Department of Physics,*
Tsinghua University, Beijing 100084, China
[2]*School of Physics, Xi'an Jiaotong University, Xi'an 710049, China*
[3]*Frontier Science Center for Quantum Information, Beijing 100084, China*

The Greenberger-Horne-Zeilinger (GHZ) state is a key resource for quantum information processing and quantum metrology. The atomic GHZ state can be generated by one-axis twisting (OAT) interaction $H_{\text{OAT}} = \chi J_z^2$ with χ the interaction strength, but it requires a long evolution time $\chi t = \pi/2$ and is thus seriously influenced by decoherence and losses. Here we propose a three-body collective-spin XYZ model which creates a GHZ-like state in a very short timescale $\chi t \sim \ln N/N$ for N particles. We show that this model can be effectively produced by applying Floquet driving to an original OAT Hamiltonian. Compared with the ideal GHZ state, the GHZ-like state generated using our model can maintain similar metrological properties reaching the Heisenberg-limited scaling, and it shows better robustness to decoherence and particle losses. This Letter opens the avenue for generating GHZ-like states with a large particle number, which holds great potential for the study of macroscopic quantum effects and for applications in quantum metrology and quantum information.

The Schrödinger cat state [1], a class of quantum superpositions of macroscopically distinct states, is crucial in investigating large-scale quantum effects [2], understanding the quantum-to-classical transition [3] and numerous applications in quantum information science [4–6] and quantum metrology [7–10]. Many efforts have been made to demonstrate such states in diverse systems, including trapped ions [11–15], photonic systems [16–23], superconducting circuits [24–27], Rydberg atoms [28], solid states [29], and so on. Some typical types of the Schrödinger cat state are especially attractive, such as the entangled coherent state of photons [30–32] and the multiparticle maximally entangled state, which is often referred to as the Greenberger-Horne-Zeilinger (GHZ) state [33] or NOON state [34]. In addition to its fundamental significance of demonstrating quantum nonlocality [33,35], the GHZ state can also be applied in quantum metrology to achieve Heisenberg-limited measurement precision [36,37], which is even better than the optimal performance of squeezed spin states [10,38–54].

To generate the GHZ state, entangling gates between quantum bits can be used [27,55–59], but the scale is very small. A large-scale GHZ state can be generated using the collective-spin one-axis twisting (OAT) model $H_{\text{OAT}} = \chi J_z^2$ [38], but the required time $\chi t = \pi/2$ is quite long, setting obstacles for realizations due to decoherence and particle losses [60–66]. Measurement and postselection can be used to shorten the evolution time at the expense of the probability of success [67]. Further studies show that by adding a turning term $\propto J_x$ to a OAT Hamiltonian, a many-particle entangled state that resembles GHZ state

can be obtained in a short timescale [68,69], but it differs from the ideal GHZ state in its wider probability distribution on the Fock-space basis.

Here we present a three-body collective-spin interaction model $H_{\text{XYZ}} \propto J_x J_y J_z + J_z J_y J_x$ (which we name the XYZ model) to rapidly create a GHZ-like state possessing a Heisenberg-limited metrological property and even being much more robust than ideal GHZ state. Using the XYZ model, the time to obtain the GHZ-like state scales as $\chi t \sim \ln N/N$, representing a great shortcut compared with the OAT model, especially for a large number of particles N. Considering practical realizations, we propose a Floquet driving scheme to effectively produce the XYZ model from an original OAT Hamiltonian. The metrological property of the obtained GHZ-like state shows a Heisenberg-limited precision in parity measurements. The degradation of the GHZ-like state due to decoherence and particle losses is much slighter than that of the ideal GHZ state, enabling its application in noisy environments.

We introduce a collective-spin cubic interaction model for N spin-$1/2$ particles, with the Hamiltonian given by

$$H_{\text{XYZ}} = \frac{2\chi_{\text{XYZ}}}{N}(J_x J_y J_z + J_z J_y J_x), \tag{1}$$

where $J_\mu = \sum_{k=1}^{N} \sigma_\mu^{(k)}/2$ ($\mu = x, y, z$) in terms of Pauli matrices $\sigma_\mu^{(k)}$ denotes the component of the collective spin operator $\mathbf{J}$ with total spin $j = N/2$, and χ_{XYZ} is the interaction strength. Since the Hamiltonian is symmetric
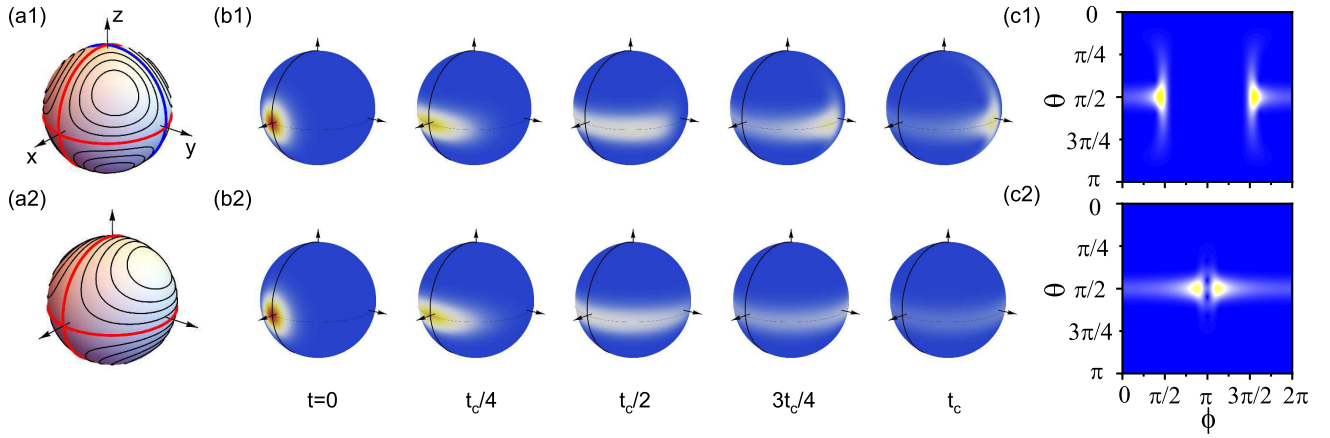
FIG. 1. Dynamics of the XYZ model and the TAT model, with $\chi_{XYZ} = \chi_{TAT}$. (a) Classical trajectories of (a1) the XYZ model and (a2) the TAT model on the Bloch sphere. The red trajectories are separatrixes shared by the XYZ model and the TAT model, while the blue one is one that only exists in the XYZ model. (b) Evolution of the quantum states of (b1) the XYZ model and (b2) the TAT model, represented by the Husimi $\mathcal{Q}$ function on the Bloch spheres. The evolution time is labeled with $t_c = \ln N/(N\chi_{XYZ})$. (c) Husimi $\mathcal{Q}$ function of (c1) the XYZ model and (c2) the TAT model at $t = t_c$, represented with polar coordinates (θ, ϕ).

under cyclic permutations of J_x, J_y, and J_z, we refer to it as the XYZ model hereafter.

As plotted in Fig. 1, starting from an initial coherent spin state $|x\rangle$ satisfying $J_x|x\rangle = j|x\rangle$, we find that the evolution under H_{XYZ} can stretch the state along the equator and split it into a GHZ-like state, a coherent superposition of two states concentrating near $(0, 1, 0)$ and $(0, -1, 0)$ on the Bloch sphere, respectively. For a short timescale before reaching the GHZ-like state, the state evolution is similar to the well-known two-axis twisting (TAT) model [38,42]
$H_{TAT} = \chi_{TAT}(J^2_{\pi/4,\pi/2} - J^2_{\pi/4,-\pi/2}) = \chi_{TAT}(J_y J_z + J_z J_y)$,
where $J_{\pi/4,\pm\pi/2} = (J_y \pm J_z)/\sqrt{2}$, corresponding to two twisting axes along $\pm 45°$ directions in the y-z plane. By comparing the semiclassical trajectories [70] as shown in Fig. 1(a), we can find that the XYZ and TAT models behave similarly near the x poles $(\pm 1, 0, 0)$ on the Bloch sphere, with the same separatrixes described by the great circles in the x-y and x-z planes (red circles); but they behave differently near the y poles $(0, \pm 1, 0)$, where the XYZ model has an additional separatrix described by the great circles in the y-z planes (blue circles), which leads to two additional fixed points at $(0, \pm 1, 0)$. Therefore, as shown in Fig. 1(b), for short t when the state is distributed near the pole $(1, 0, 0)$, the evolution under the XYZ model resembles the TAT model with the stretch of the state along the equator, but the evolutions diverge for longer time. For the TAT model, the state evolution will cross over the points $(0, \pm 1, 0)$ and finally converge near the point $(-1, 0, 0)$ $(\phi = \pi)$, while for the XYZ model, the state distribution can be split into two symmetric parts near the fixed points $(0, \pm 1, 0)$, as it sets stoppages at these fixed points. The comparison is shown more clearly in

Fig. 1(c), where the state in the XYZ model is located near $(\theta, \phi) = (\pi/2, \pi/2)$ and $(\pi/2, 3\pi/2)$ in the polar coordinates, with the separation reaching the maximum.

To obtain the critical evolution time for generating the GHZ-like state in the XYZ model, we can use the semiclassical treatment by considering the evolution of the point at the edge of the uncertainty patch [70,71], which approximately yields

$$t_c \simeq \frac{\ln N}{\chi_{XYZ}N}. \tag{2}$$

It reveals that the required time can be very short for large particle number N, far less than that of the OAT dynamics, which is of crucial importance for overcoming decoherence and losses.

The proposed XYZ model may be difficult to find directly in existing systems, as the collective-spin cubic Hamiltonian requires three-particle interaction. In light of this, we propose a Floquet-driving scheme to synthesize the XYZ model from an original OAT interaction $H_{OAT} = \chi J^2_z$ which commonly exists in many realistic systems [72–76]. The scheme utilizes periodic $\pm\pi/2$ pulses along the α axis with $R^{\alpha}_{\pm\pi/2} = e^{\mp i\pi J_\alpha/2}$ $(\alpha = x, y)$. Each period is 3τ and is made up of the following: two $\pm\pi/2$ rotations about x axis separated by a free evolution for τ, two $\pm\pi/2$ rotations about y axis separated by a second free evolution for τ, and a third free evolution for τ. This is a special case of the general time-dependent Hamiltonian $H(t) = \Omega_x(t)J_x + \Omega_y(t)J_y + H_{OAT}$ with $\Omega_\alpha(t)$ consisting of a series of Dirac delta functions, which means the duration of driving pulses is short enough to be ignored, as illustrated in Fig. 2(a). The evolution operator
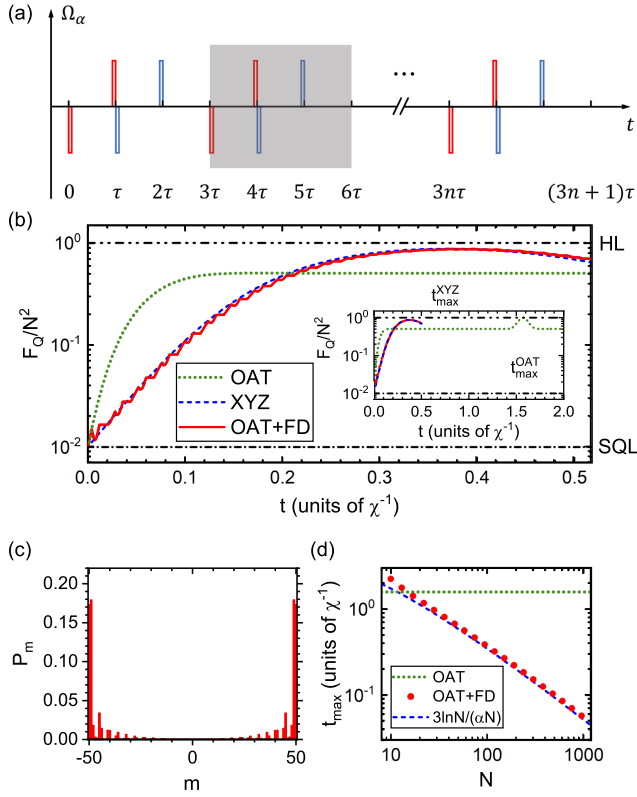
FIG. 2. Generation of the catlike state with Floquet driving. (a) An illustration of the proposed pulse sequences. One period is 3τ (shaded), consisting of $\pm\pi/2$ pulses (up for "+" and down for "−") along the x axis (red one) and y axis (blue one). (b) Time evolution of the optimal quantum Fisher information F_Q of the original OAT model (green dotted), the effective XYZ model (blue dashed), and the proposed Floquet-driving scheme with driving parameter $\alpha = 0.4$ (red solid) for $N = 100$ particles. Horizontal lines indicate the standard quantum limit $F_Q = N$ (black dash-dotted line) and the Heisenberg limit $F_Q = N^2$ (black dash-dot-dotted line). The time when F_Q reaches its maximum of the XYZ model and the OAT model are marked as $t_{\max}^{XYZ}$ and $t_{\max}^{OAT}$, respectively. (c) Probability distribution $P_m = |\langle m|\psi\rangle|^2$ on eigenstates of J_y at $t = t_{\max}^{XYZ}$ for the XYZ model. (d) Optimal time $t_{\max}$ when F_Q reaches its maximum for the OAT model (green dotted) and the proposed Floquet-driving scheme (red circles) versus particle number N, compared with the predicted value $t_c \simeq 3\ln N/(\alpha N)$ (blue dashed line).

for one period can be written as

$$U = e^{-i\chi J_z^2\tau}R_{\pi/2}^y e^{-i\chi J_z^2\tau}R_{-\pi/2}^y R_{\pi/2}^x e^{-i\chi J_z^2\tau}R_{-\pi/2}^x$$
$$= e^{-i\chi J_z^2\tau}e^{-i\chi J_x^2\tau}e^{-i\chi J_y^2\tau}. \tag{3}$$

We can find that the driving pulses transform the original one-axis twisting into sequential three-axis twisting. Although the first order terms vanish as $J_x^2 + J_x^2 + J_x^2 = j(j+1)$ is a constant, the second order terms are not canceled due to the noncommutativity of the operators. We simplify the expression using the Baker-Campbell-Hausdorff formula, which

results in [70]

$$U = \exp\left[-i\chi^2\tau^2(J_xJ_yJ_z + J_zJ_yJ_x) + \mathcal{O}(\tau^2)\right]. \tag{4}$$

For small τ ($\chi\tau N/2 \ll 1$), we can ignore the higher order terms and arrive at $U \simeq e^{-i\chi^2\tau^2(J_xJ_yJ_z+J_zJ_yJ_x)}$, and the corresponding effective Hamiltonian becomes

$$H_{\text{eff}} = \frac{1}{3}\chi^2\tau(J_xJ_yJ_z + J_zJ_yJ_x), \tag{5}$$

which has exactly the form of the XYZ model (1), with effective interaction strength $\chi_{XYZ}^{\text{eff}} = \chi^2\tau N/6$. To safely drop higher order terms, we may set $\chi\tau = 2\alpha/N$ with $\alpha \lesssim 1$ being an alternative driving parameter. The effective interaction strength then reads $\chi_{XYZ}^{\text{eff}} = \alpha\chi/3$. We mention that an interaction strength with opposite sign can be obtained by simply adjusting the order of pulse sequences.

To verify the validity of the Floquet-driving scheme, in Fig. 2(b) we plot the time evolution of the optimal quantum Fisher information (QFI) in the Floquet-driving scheme, compared with the dynamics of the original OAT model and the effective XYZ model. Assuming a phase ϕ is encoded via $e^{-iJ_n\phi}$ to an input state $\hat{\rho}_0$, the QFI can be expressed as

$$F_Q(\hat{\rho}_0, J_{\mathbf{n}}) = 2\sum_{q_\kappa+q_{\kappa'}>0}\frac{(q_\kappa - q_{\kappa'})^2}{q_\kappa + q_{\kappa'}}|\langle\kappa'|J_{\mathbf{n}}|\kappa\rangle|^2, \tag{6}$$

where $\hat{\rho}_0 = \sum_\kappa q_\kappa|\kappa\rangle\langle\kappa|$ represents the spectral decomposition of the input state. The QFI is bounded by the Heisenberg limit $F_Q(|\hat{\rho}_0\rangle, J_{\mathbf{n}}) \leq N^2$ for N particles. For a pure input state $\hat{\rho}_0 = |\psi_0\rangle\langle\psi_0|$, the expression is reduced to $F_Q(|\psi_0\rangle, J_{\mathbf{n}}) = 4(\Delta J_{\mathbf{n}})^2$. From Fig. 2(b) we can find that for the Floquet-driving scheme, the QFI can approach the Heisenberg limit in a fairly short time, in good accordance with the result of the effective XYZ model. Compared with the OAT dynamics which achieves the Heisenberg limit at $\chi t = \pi/2$, the time required in our scheme is greatly shortened.

At $t = t_{\max}^{XYZ}$ when F_Q achieves its maximum for the XYZ model, the probability distribution on eigenstates of J_y ($\{|m\rangle_y\}_{m=-N/2}^{N/2}$, $J_y|m\rangle_y = m|m\rangle_y$) is shown in Fig. 2(c). We find that the distribution is perfectly symmetric for $\pm m$, with about 70% of the population on $m = \pm N/2$ and $\pm(N/2 - 1)$, which resembles the GHZ state to a large extent. Note that this distribution is much more concentrated than the state created through twist-and-turn dynamics [70]. The required generation time for different particle numbers is plotted in Fig. 2(d). The result matches well with the predicted value $t_c \simeq \ln N/(\chi_{\text{eff}}N) = 3\ln N/(\alpha N\chi)$.

A characteristic behavior of the GHZ state is the fast oscillation of parity [13,28,36,37], defined as $\Pi = \sum_m(-1)^m|m\rangle\langle m|$ ($|m\rangle$ is the Dicke state with $J_z|m\rangle = m|m\rangle$), after applying a $\pi/2$ rotation $e^{i\pi J_\theta/2}$ where
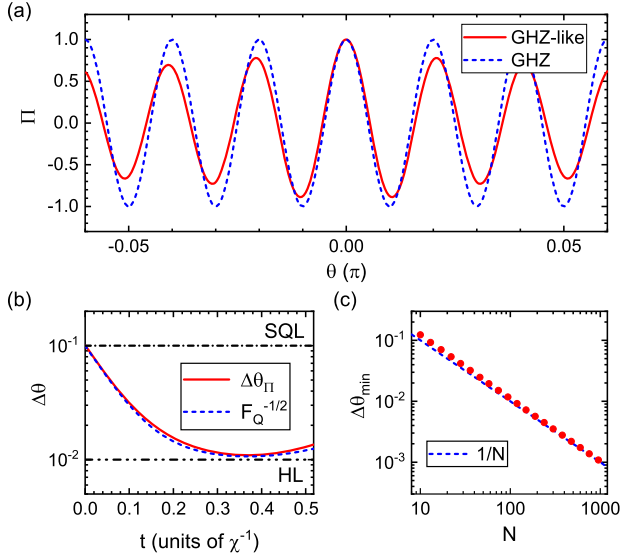
FIG. 3. Parity oscillation of the GHZ-like state for $N = 100$ particles. (a) The expectation value of parity Π versus the azimuth angle θ of the rotation axis, for the GHZ-like state generated through the XYZ dynamics (red solid line) and the perfect GHZ state (black dashed line). (b) The precision $\Delta\theta$ at $\theta_0 = \pi/(2N)$ versus evolution time t of the XYZ dynamics (red solid line), in comparison with the quantum Cramér-Rao bound $F_Q^{-1/2}$ (blue dashed line). (c) The optimal precision $\Delta\theta_{\min}$ versus particle number N of the GHZ-like state (red circles), comparing with the Heisenberg limit $1/N$ (blue dashed line).
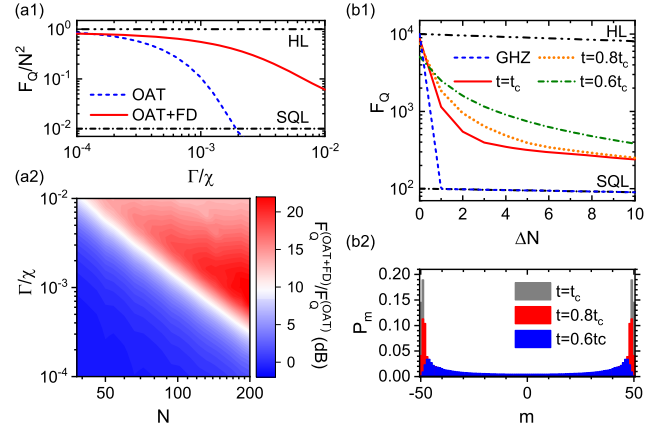

FIG. 4. The effective XYZ dynamics and the obtained GHZ-like state in the presence of decoherence and losses. (a1) The quantum Fisher information F_Q of the GHZ(-like) state created through our Floquet-driving scheme (red solid line) and OAT dynamics (blue dashed line) for $N = 100$ particles with respect to Γ. (a2) The ratio of the quantum Fisher information for two dynamics $F_Q^{(\mathrm{OAT+FD})}/F_Q^{(\mathrm{OAT})}$ versus N and Γ. Data are calculated at $\chi t = 3 \ln N/(\alpha N)$ with $\alpha = 0.4$ for Floquet-driving scheme and $\chi t = \pi/2$ for OAT scheme. (b1) The optimal quantum Fisher information of the perfect GHZ state (blue dashed line) and the GHZ-like state generated through XYZ dynamics at $t = t_c$ (red solid line), $t = 0.8t_c$ (orange dotted), and $t = 0.6t_c$ (green dash-dotted line) when ΔN particles are lost. (b2) The probability distribution P_m for the GHZ-like state generated through XYZ dynamics at $t = t_c$ (gray), $t = 0.8t_c$ (red) and $t = 0.6t_c$ (blue).

$J_\theta = J_y \cos\theta - J_x \sin\theta$. This property is also possessed by the GHZ-like state generated through the XYZ dynamics. In Fig. 3(a) we plot the expectation value of parity with respect to θ. For a perfect GHZ state $|\mathrm{GHZ}\rangle = (|N/2\rangle + |-N/2\rangle)/\sqrt{2}$, the parity oscillation can be derived analytically as $\Pi(\theta) = \cos(N\theta)$. For the generated GHZ-like state [concentrating at $(0, 0, \pm 1)$ on the Bloch sphere], we can see that the result resembles that of the GHZ state, verifying its GHZ-like property. The components other than $m = \pm N/2$ in the GHZ-like state will degrade the amplitude of oscillation only when θ becomes larger.

The high-frequency oscillation of parity can be applied in high-precision measurement to obtain a precision approaching the Heisenberg limit $\Delta\theta_{\mathrm{HL}} = 1/N$. We choose $\theta_0 = \pi/(2N)$ where the gradient $|\partial_\theta \Pi|$ nearly reaches its maximum and calculate the precision as $\Delta\theta = |\Delta\Pi/\partial_\theta \Pi|_{\theta=\theta_0}$. Figure 3(b) shows the result obtained with an input state which evolves under H_{XYZ} for t from an initial coherent spin state $|x\rangle$. We find the precision is always approaching the quantum Cramér-Rao bound $\Delta\theta_{\mathrm{QCRB}} = F_Q^{-1/2}$, which means the parity measurement is always an ideal one to exploit the metrology-enhanced property generated by the XYZ model [70]. The optimal precision $\Delta\theta_{\min}$ versus particle number N is plotted in Fig. 3(c), proving a Heisenberg-limited precision.

To analyze the impact of decoherence, we consider the effective OAT interaction mediated by an optical cavity as proposed in Ref. [75]. In such schemes the cavity mode couples the ground $|\downarrow\rangle \equiv {}^1S_0$ and excited $|\uparrow\rangle \equiv {}^3P_0$ clock states of ^{87}Sr atoms, leading to the effective OAT Hamiltonian $H_{\mathrm{eff}} = \chi(J^2 - J_z^2)$, accompanied with an effective Lindblad operator $L = \sqrt{\Gamma/2}J_-$ which describes the superradiance caused by the leakage of photons out of the cavity. In Figs. 4(a1) and 4(a2) we examine the effects of this typical decoherence channel on the creation of GHZ (-like) states. Since our Floquet-driving scheme greatly shortens the evolution time, it is reasonable to find that it outperforms the OAT scheme as the intensity of superradiance Γ gets larger. The ratio of the QFI for two schemes $F_Q^{\mathrm{OAT+FD}}/F_Q^{\mathrm{OAT}}$ is plotted in Fig. 4(a2), which further confirms the superiority of our scheme in the case of a large particle number, owing to the $\ln N/N$ dependence of the evolution time. One may notice that for large N, this ratio slightly drops after its first rise as Γ grows. This is simplify the consequence that the OAT dynamics has been almost completely destroyed by the severe effect of decoherence, making F_Q^{OAT} nearly unchanged as Γ continues to increase.

The GHZ state is also known to be extremely fragile to losses, with its coherence completely destroyed when only

one particle is lost, while our GHZ-like state is more robust. In Fig. 4(b1) we compare the performance of the GHZ-like states with the perfect GHZ state in the presence of particle losses. The degradation of the QFI for the GHZ-like states is slighter than that of the perfect GHZ state, which can be further improved by shortening the evolution time and using a GHZ-like state with a wider probability distribution, as illustrated by the examples of $t = 0.8t_c$ and $0.6t_c$ in Figs. 4(b1) and 4(b2). This can be interpreted as the wider distribution ensuring more coherence lying in the matrix elements $|\pm(N/2 - n)\rangle\langle\mp(N/2 - n)|$, which survives after $n \geq 1$ particles are lost. We note that the QFI of the GHZ-like states seems to asymptotically stable to a fixed value above the standard quantum limit when the number of lost particles ΔN is large, indicating that each one of the two parts of the GHZ-like state is still non-classical and possesses metrologically useful properties.

In conclusion, we present a three-body collective-spin XYZ model to rapidly create GHZ-like states. It shows a significant shortcut of timescale from $\chi t = \pi/2$ of the OAT model to $\chi t \sim \ln N/N$ of our model. We proposed to realize the XYZ model by employing Floquet driving to an original OAT interaction. We further study the behavior of GHZ-like states in parity measurements, and obtain a Heisenberg-limited level of measurement precision, showing that the metrology-enhanced property of the XYZ model can be always fully exploited by taking parity measurements. Moreover, we investigate the behavior of our scheme and the obtained GHZ-like state in the presence of decoherence and losses, finding it more robust than the OAT scheme and the ideal GHZ state. Our Letter paves the way for the creation of large-particle-number GHZ-like states, which has significant applications in quantum metrology and quantum information science.

---

*These authors contributed equally to this work.
†ycliu@tsinghua.edu.cn

[1] E. Schrödinger, Naturwissenschaften **23**, 844 (1935).
[2] F. Fröwis, P. Sekatski, W. Dür, N. Gisin, and N. Sangouard, Rev. Mod. Phys. **90**, 025004 (2018).
[3] M. Brune, E. Hagley, J. Dreyer, X. Maître, A. Maali, C. Wunderlich, J. M. Raimond, and S. Haroche, Phys. Rev. Lett. **77**, 4887 (1996).
[4] Z. Zhao, Y. Chen, A. Zhang, T. Yang, H. Briegel, and J. Pan, Nature (London) **430**, 54 (2004).
[5] E. Knill, Nature (London) **434**, 39 (2005).
[6] M. Mirrahimi, Z. Leghtas, V. V. Albert, S. Touzard, R. J. Schoelkopf, L. Jiang, and M. H. Devoret, New J. Phys. **16**, 045014 (2014).
[7] W. J. Munro, K. Nemoto, G. J. Milburn, and S. L. Braunstein, Phys. Rev. A **66**, 023819 (2002).
[8] V. Giovannetti, S. Lloyd, and L. Maccone, Science **306**, 1330 (2004).
[9] C. L. Degen, F. Reinhard, and P. Cappellaro, Rev. Mod. Phys. **89**, 035002 (2017).
[10] L. Pezzè, A. Smerzi, M. K. Oberthaler, R. Schmied, and P. Treutlein, Rev. Mod. Phys. **90**, 035005 (2018).
[11] D. J. Wineland, Rev. Mod. Phys. **85**, 1103 (2013).
[12] C. Monroe, D. M. Meekhof, B. E. King, and D. J. Wineland, Science **272**, 1131 (1996).
[13] C. Sackett, D. Kielpinski, B. King, C. Langer, V. Meyer, C. Myatt, M. Rowe, Q. Turchette, W. Itano, D. Wineland, and C. Monroe, Nature (London) **404**, 256 (2000).
[14] T. Monz, P. Schindler, J. T. Barreiro, M. Chwalla, D. Nigg, W. A. Coish, M. Harlander, W. Hänsel, M. Hennrich, and R. Blatt, Phys. Rev. Lett. **106**, 130506 (2011).
[15] H.-Y. Lo, D. Kienzler, L. de Clercq, M. Marinelli, V. Negnevitsky, B. C. Keitch, and J. P. Home, Nature (London) **521**, 336 (2015).
[16] A. Ourjoumtsev, R. Tualle-Brouri, J. Laurat, and P. Grangier, Science **312**, 83 (2006).
[17] S. Deleglise, I. Dotsenko, C. Sayrin, J. Bernu, M. Brune, J.-M. Raimond, and S. Haroche, Nature (London) **455**, 510 (2008).
[18] W.-B. Gao, C.-Y. Lu, X.-C. Yao, P. Xu, O. Guehne, A. Goebel, Y.-A. Chen, C.-Z. Peng, Z.-B. Chen, and J.-W. Pan, Nat. Phys. **6**, 331 (2010).
[19] K. Huang, H. Le Jeannic, J. Ruaudel, V. B. Verma, M. D. Shaw, F. Marsili, S. W. Nam, E. Wu, H. Zeng, Y.-C. Jeong, R. Filip, O. Morin, and J. Laurat, Phys. Rev. Lett. **115**, 023602 (2015).
[20] C. Wang, Y. Y. Gao, P. Reinhold, R. W. Heeres, N. Ofek, K. Chou, C. Axline, M. Reagor, J. Blumoff, K. M. Sliwa, L. Frunzio, S. M. Girvin, L. Jiang, M. Mirrahimi, M. H. Devoret, and R. J. Schoelkopf, Science **352**, 1087 (2016).
[21] D. V. Sychev, A. E. Ulanov, A. A. Pushkina, M. W. Richards, I. A. Fedorov, and A. I. Lvovsky, Nat. Photonics **11**, 379 (2017).
[22] B. Hacker, S. Welte, S. Daiss, A. Shaukat, S. Ritter, L. Li, and G. Rempe, Nat. Photonics **13**, 110 (2019).
[23] Z. Wang, Z. Bao, Y. Wu, Y. Li, W. Cai, W. Wang, Y. Ma, T. Cai, X. Han, J. Wang, Y. Song, L. Sun, H. Zhang, and L. Duan, Sci. Adv. **8**, eabn1778 (2022).
[24] J. Friedman, V. Patel, W. Chen, S. Tolpygo, and J. Lukens, Nature (London) **406**, 43 (2000).
[25] L. DiCarlo, M. D. Reed, L. Sun, B. R. Johnson, J. M. Chow, J. M. Gambetta, L. Frunzio, S. M. Girvin, M. H. Devoret, and R. J. Schoelkopf, Nature (London) **467**, 574 (2010).
[26] C. Song, K. Xu, W. Liu, C. P. Yang, S. B. Zheng, H. Deng, Q. Xie, K. Huang, Q. Guo, L. Zhang, P. Zhang, D. Xu, D. Zheng, X. Zhu, H. Wang, Y.-A. Chen, C.-Y. Lu, S. Han, and J.-W. Pan, Phys. Rev. Lett. **119**, 180511 (2017).
[27] C. Song, K. Xu, H. Li, Y.-R. Zhang, X. Zhang, W. Liu, Q. Guo, Z. Wang, W. Ren, J. Hao, H. Feng, H. Fan, D. Zheng, D.-W. Wang, H. Wang, and S.-Y. Zhu, Science **365**, 574 (2019).
[28] A. Omran, H. Levine, A. Keesling, G. Semeghini, T. T. Wang, S. Ebadi, H. Bernien, A. S. Zibrov, H. Pichler, S. Choi, J. Cui, M. Rossignolo, P. Rembold, S. Montangero,

T. Calarco, M. Endres, M. Greiner, V. Vuletić, and M. D. Lukin, Science **365**, 570 (2019).

[29] M. Bild, M. Fadel, Y. Yang, U. von Lüpke, P. Martin, A. Bruno, and Y. Chu, Science **380**, 274 (2023).

[30] J. Joo, W. J. Munro, and T. P. Spiller, Phys. Rev. Lett. **107**, 083601 (2011).

[31] B. C. Sanders, J. Phys. A **45**, 244002 (2012).

[32] Y. M. Zhang, X. W. Li, W. Yang, and G. R. Jin, Phys. Rev. A **88**, 043832 (2013).

[33] D. Greenberger, M. Horne, A. Shimony, and A. Zeilinger, Am. J. Phys. **58**, 1131 (1990).

[34] H. Lee, P. Kok, and J. P. Dowling, J. Mod. Opt. **49**, 2325 (2002).

[35] N. D. Mermin, Phys. Rev. Lett. **65**, 1838 (1990).

[36] J. J. Bollinger, W. M. Itano, D. J. Wineland, and D. J. Heinzen, Phys. Rev. A **54**, R4649 (1996).

[37] D. Leibfried, M. Barrett, T. Schaetz, J. Britton, J. Chiaverini, W. Itano, J. Jost, C. Langer, and D. Wineland, Science **304**, 1476 (2004).

[38] M. Kitagawa and M. Ueda, Phys. Rev. A **47**, 5138 (1993).

[39] D. J. Wineland, J. J. Bollinger, W. M. Itano, and D. J. Heinzen, Phys. Rev. A **50**, 67 (1994).

[40] A. S. Sørensen and K. Mølmer, Phys. Rev. Lett. **86**, 4431 (2001).

[41] G.-R. Jin, Y.-C. Liu, and W.-M. Liu, New J. Phys. **11**, 073049 (2009).

[42] Y. C. Liu, Z. F. Xu, G. R. Jin, and L. You, Phys. Rev. Lett. **107**, 013601 (2011).

[43] J. Ma, X. Wang, C. Sun, and F. Nori, Phys. Rep. **509**, 89 (2011).

[44] C. Shen and L.-M. Duan, Phys. Rev. A **87**, 051801(R) (2013).

[45] J.-Y. Zhang, X.-F. Zhou, G.-C. Guo, and Z.-W. Zhou, Phys. Rev. A **90**, 013604 (2014).

[46] F. Chen, J.-J. Chen, L.-N. Wu, Y.-C. Liu, and L. You, Phys. Rev. A **100**, 041801(R) (2019).

[47] L.-G. Huang, F. Chen, X. Li, Y. Li, R. Lu, and Y.-C. Liu, npj Quantum Inf. **7**, 168 (2021).

[48] Z. Hu, Q. Li, X. Zhang, L.-G. Huang, H. B. Zhang, and Y.-C. Liu, Phys. Rev. A **108**, 023722 (2023).

[49] L.-G. Huang, X. Zhang, Y. Wang, Z. Hua, Y. Tang, and Y.-C. Liu, Phys. Rev. A **107**, 042613 (2023).

[50] G. Bornet, G. Emperauger, C. Chen, B. Ye, M. Block, M. Bintz, J. A. Boyd, D. Barredo, T. Comparin, F. Mezzacapo, T. Roscilde, T. Lahaye, N. Y. Yao, and A. Browaeys, Nature (London) **621**, 728 (2023).

[51] C. K. Law, H. T. Ng, and P. T. Leung, Phys. Rev. A **63**, 055601 (2001).

[52] H. Strobel, W. Muessel, D. Linnemann, T. Zibold, D. B. Hume, L. Pezzè, A. Smerzi, and M. K. Oberthaler, Science **345**, 424 (2014).

[53] W. Muessel, H. Strobel, D. Linnemann, T. Zibold, B. Juliá-Díaz, and M. K. Oberthaler, Phys. Rev. A **92**, 023603 (2015).

[54] G. Sorelli, M. Gessner, A. Smerzi, and L. Pezzè, Phys. Rev. A **99**, 022329 (2019).

[55] T. Choi, S. Debnath, T. A. Manning, C. Figgatt, Z.-X. Gong, L.-M. Duan, and C. Monroe, Phys. Rev. Lett. **112**, 190502 (2014).

[56] R. Barends *et al.*, Nature (London) **508**, 500 (2014).

[57] H. Kaufmann, T. Ruster, C. T. Schmiegelow, M. A. Luda, V. Kaushal, J. Schulz, D. von Lindenfels, F. Schmidt-Kaler, and U. G. Poschinger, Phys. Rev. Lett. **119**, 150503 (2017).

[58] Y. Lu, S. Zhang, K. Zhang, W. Chen, Y. Shen, J. Zhang, J.-N. Zhang, and K. Kim, Nature (London) **572**, 363 (2019).

[59] K. X. Wei, I. Lauer, S. Srinivasan, N. Sundaresan, D. T. McClure, D. Toyli, D. C. McKay, J. M. Gambetta, and S. Sheldon, Phys. Rev. A **101**, 032343 (2020).

[60] A. Sorensen, L. Duan, J. Cirac, and P. Zoller, Nature (London) **409**, 63 (2001).

[61] L. Pezzè and A. Smerzi, Phys. Rev. Lett. **102**, 100401 (2009).

[62] G. S. Agarwal, R. R. Puri, and R. P. Singh, Phys. Rev. A **56**, 2249 (1997).

[63] K. Mølmer and A. Sørensen, Phys. Rev. Lett. **82**, 1835 (1999).

[64] S.-B. Zheng, Phys. Rev. Lett. **87**, 230404 (2001).

[65] D. Leibfried, E. Knill, S. Seidelin, J. Britton, R. Blakestad, J. Chiaverini, D. Hume, W. Itano, J. Jost, C. Langer, R. Ozeri, R. Reichle, and D. Wineland, Nature (London) **438**, 639 (2005).

[66] T. Chalopin, C. Bouazza, A. Evrard, V. Makhalov, D. Dreon, J. Dalibard, L. A. Sidorenkov, and S. Nascimbene, Nat. Commun. **9**, 4955 (2018).

[67] B. Alexander, J. J. Bollinger, and H. Uys, Phys. Rev. A **101**, 062303 (2020).

[68] A. Micheli, D. Jaksch, J. I. Cirac, and P. Zoller, Phys. Rev. A **67**, 013607 (2003).

[69] Y. P. Huang and M. G. Moore, Phys. Rev. A **73**, 023606 (2006).

[70] See Supplemental Material at http://link.aps.org/supplemental/10.1103/PhysRevLett.132.113402 for details.

[71] M. H. Muñoz-Arias, I. H. Deutsch, and P. M. Poggi, PRX Quantum **4**, 020314 (2023).

[72] C. Gross, T. Zibold, E. Nicklas, J. Esteve, and M. K. Oberthaler, Nature (London) **464**, 1165 (2010).

[73] M. F. Riedel, P. Boehi, Y. Li, T. W. Haensch, A. Sinatra, and P. Treutlein, Nature (London) **464**, 1170 (2010).

[74] I. D. Leroux, M. H. Schleier-Smith, and V. Vuletić, Phys. Rev. Lett. **104**, 073602 (2010).

[75] M. A. Norcia, R. J. Lewis-Swan, J. R. K. Cline, B. Zhu, A. M. Rey, and J. K. Thompson, Science **361**, 259 (2018).

[76] J. A. Hines, S. V. Rajagopal, G. L. Moreau, M. D. Wahrman, N. A. Lewis, O. Marković, and M. Schleier-Smith, Phys. Rev. Lett. **131**, 063401 (2023).